Electro-osmosis in a nanometer-scale channel studied by atomistic simulation

Jonathan B. Freund[a)]
Theoretical and Applied Mechanics, University of Illinois at Urbana-Champaign, Urbana, Illinois 61801

(Received 27 August 2001; accepted 8 November 2001)

An atomistic simulation of an electro-osmotic flow in a 65.3 Å-wide channel is performed to study its physical details and evaluate continuum models. The working fluid is a 0.01 M solution (at midchannel) of Cl^- in water. For simplicity and computational efficiency, only negatively charged ions are included. The water is modeled by the SPC/E potential and the Cl^- are modeled as point charges plus an established Lennard-Jones potential. The channel walls are fixed lattices of positively charged Lennard-Jones atoms. In one case an appropriate fraction of the wall atoms is given elementary charges; for comparison, another case is simulated with uniformly distributed partial charges on the wall atoms. For the distributed elementary charge case the Cl^- concentration at the wall is 80 percent higher than predicted by the Poisson–Boltzmann theory. It is over 100 percent higher for the uniformly charged wall case. In both cases, the waters in the 10 Å closest to the walls are preferentially oriented. Their respective orientations are similar except in the first monolayer. However, the effect of this orientational bias on the permittivity and subsequently the Cl^- distribution is shown to be minor by Monte Carlo simulations, which predict an ion distribution in agreement with the dynamic simulation using only $\varepsilon = 80$ to model the water. Computed, one-dimensional self-diffusivities of the waters match accepted values greater than 10 Å from the walls, but decay significantly close to the walls. The decay is not monotonic for the wall-normal diffusivity. The atoms near the walls are not fixed in a Stern layer, as typically assumed in models, but the viscosity is found to increase by over a factor of 6 in the 10 Å closest to the wall. © *2002 American Institute of Physics.* [DOI: 10.1063/1.1431543]

I. INTRODUCTION

Where an electrolyte contacts a solid surface it is common that the surface becomes charged, with negative counter ions preferentially distributed above it in an electric double layer (see Fig. 1). The ion density in this charged layer is typically modeled by a Boltzmann distribution. To ease computational expense, in the present study we only have negative counter ions in the fluid between positively charged walls, so the ion number density is simply

$$n(y) = n_0 e^{e\phi(y)/k_B T}, \tag{1}$$

where T is the temperature of the fluid (assumed uniform), k_B is the Boltzmann constant, e is the elementary charge (positive), and ϕ is the local electric potential, which is a function of the wall-normal coordinate y. We choose the midchannel potential $\phi(y=y_m)=0$, so $n_0 = n(y_m)$. The electric potential in (1) satisfies the one-dimensional Poisson–Boltzmann equation

$$\frac{d^2\phi}{dy^2} = \frac{en(y)}{\varepsilon\varepsilon_0} = \frac{en_0}{\varepsilon\varepsilon_0} e^{e\phi(y)/k_B T}, \tag{2}$$

where ε_0 is the permittivity of a vacuum and ε (assumed constant) parametrizes the dielectric behavior of the fluid. We have assumed monovalent ions. The solution of (2) is[1]

$$\phi(y) = -\frac{k_B T}{e} \log\left[\cos^2 \sqrt{\frac{e^2 n_0 (y-y_m)^2}{2\varepsilon\varepsilon_0 k_B T}}\right]. \tag{3}$$

Overall electroneutrality gives a boundary condition on ϕ in terms of the wall charge density Q_0

$$Q_0 = \varepsilon\varepsilon_0 \left.\frac{d\phi}{dy}\right|_{\text{walls}}, \tag{4}$$

which can be used to determine n_0. One objective of this study is to examine the reliability of constant ε for this flow. For polar solvents deviation is expected since the strong electric field in the neighborhood of the walls will alter the response of the solvent to $\nabla\phi$ in this region. Some relevant experiments are reviewed by Hunter.[2]

Typically, the fluid molecules nearest the wall are assumed to be bound to the surface in the so-called Stern layer. Beyond the Stern layer, the fluid will flow under the influence of an applied electric field E. This electrokinetic flow is known as electro-osmosis. The flowing and fixed regions are usually assumed to be separated by a shear plane, a no-slip boundary condition applied at a finite distance above the wall, but since the Stern layer may be only a few atoms thick, a continuum model may not be accurate. Given the number density distribution in the channel from (1), the flow in the continuum model is governed by the one-dimensional Stokes equation

a)Electronic mail: jbfreund@uiuc.edu

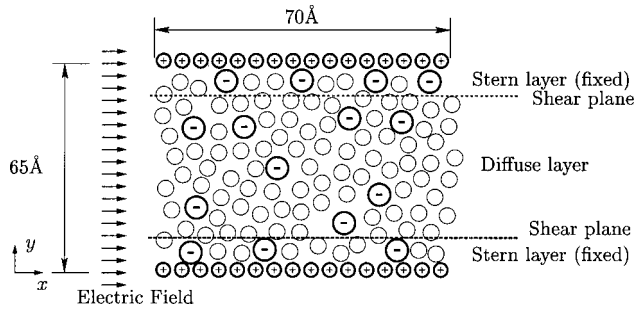

FIG. 1. Schematic of the electric double layer in a nanometer-scale channel. For simplicity, both this schematic and the present simulations only have counterions in the solution. Two dimensions of the simulated channel are labeled. It also extends 70 Å in the *z*-direction.

$$\frac{d}{dy}\left(\mu\frac{du}{dy}\right)+en(y)E=0, \tag{5}$$

where we have assumed zero pressure gradient. The viscosity μ is typically assumed to be constant.

Electro-osmosis is used to pump fluid in microfluidic devices (e.g., Herr *et al.*[3]) and to move fluid through porous material and clays (e.g., Coelho *et al.*[4]). It is also used in conjunction with theories similar to the one presented above to deduce the ζ potential, the electric potential at the supposed shear plane, which also factors into models for electrophoresis and other electrokinetic flows. Thus, the correctness of these models is also important for making these measurements.

Although the theory presented above is well established and predicts the observed gross phenomenology, the small length scales of the process make it difficult to test electro-osmosis models in detail, in particular whether or not permittivity $\varepsilon\varepsilon_0$ and viscosity μ deviate from their values in bulk or if there is noncontinuum behavior. For this reason we have developed the capability of simulating the process atomistically. Though this approach does allow us to examine in detail the dynamics of the near-wall region, it is, of course, limited to nanometer-scale channels and pores, which are significantly smaller than in present day manufactured devices. However, in many cases the double layers are indeed of nanometer scale and can therefore be studied directly by atomistic simulation. The model we examine has water with dissolved negative ions flowing in between atomically smooth solid surfaces. The interatomic potentials are modeled with the established empirical models discussed in Sec. II. This section also discusses the numerical methods, the flow parameters, and the simulation procedure. Section III presents and discusses simulation results and makes comparisons with theoretical predictions. A brief summary is provided in Sec. IV.

II. ATOMISTIC SIMULATIONS

A. Physical model

The waters were modeled using the SPC/E model,[5] which represents hydrogens and oxygens as point charges ($q_H=+0.4258e$ and $q_O=-0.8476e$). The oxygens also interact with other atoms by a Lennard-Jones potential. Tests in a nanometer-scale Couette flow showed that the SPC/E model-predicted viscosity of water at $T=300$ K was 10 percent below the accepted value, which is acceptable since the SPC/E model was not tuned to represent viscosity. The Cl^- were modeled using the parameters of Chandrasekhar *et al.*,[6] and the walls were modeled by fixed square arrays of Lennard-Jones atoms. Parameters for all Lennard-Jones interactions are given in Table I. Note that the wall–oxygen and wall–chloride interactions had the same energy.

B. Numerical method

A standard velocity Verlet algorithm was used to integrate Newton's equation of motion with a numerical time step of 1 fs. Lennard-Jones interactions were computed point-to-point using a cutoff of $2.5\sigma_{\max}$, where $\sigma_{\max}$ is the maximum σ value for all the interactions (see Table I); Coulomb interactions were computed using an aperiodic implementation[7] of the P^3M algorithm.[8] A matrix constraint method fixed the bond lengths and angles of the waters as specified by the SPC/E model.

A method like P^3M that does not truncate the Coulomb interactions is essential for these simulations since the principal phenomenology depends intrinsically upon the long-range interaction of the ions with the walls and each other. The mesh for the elliptic solver in the P^3M implementation had $64\times160\times64$ points in *x*, *y*, and *z*, respectively, with the same uniform mesh spacing in all three coordinate directions. The 160 mesh points in the *y* direction extended over twice the height of the channel and were used in conjunction with an appropriately modified influence function to remove the periodicity.[7] In our implementation, the point-to-point and mesh portions of the potential were split using the standard Ewald decomposition

TABLE I. All parameters for the Lennard-Jones potential. For convenience, two equivalent forms are given: $U(r)=A/r^{12}-C/r^6$ and $U(r)=4\epsilon(\sigma^{12}/r^{12}-\sigma^6/r^6)$. The final column lists r_0, the separation distance corresponding to zero force. All Lennard-Jones potentials were cut off and shifted at the standard $r_c=2.5\sigma_{\max}$.

Interaction	A (J Å^{12})	C (J Å^6)	ϵ (J)	σ (Å)	r_0 (Å)
O–O	4.37×10^{-15}	4.35×10^{-18}	1.08×10^{-21}	3.17	3.55
Cl–O	6.75×10^{-14}	1.03×10^{-17}	3.93×10^{-22}	4.33	4.86
Cl–Cl	1.81×10^{-13}	2.43×10^{-17}	8.16×10^{-22}	4.42	4.96
W–O	3.00×10^{-14}	3.09×10^{-17}	7.95×10^{-21}	3.15	3.53
W–Cl	1.14×10^{-12}	1.90×10^{-16}	7.95×10^{-21}	4.26	4.78

$$\mathbf{F}_i = -\frac{1}{2}\sum_{i\neq j}\frac{q_i q_j}{4\pi\varepsilon_0}\left(\frac{2\alpha e^{-\alpha^2|\mathbf{x}_{ij}|^2}}{\sqrt{\pi}|\mathbf{x}_{ij}|}+\frac{\operatorname{erfc}(\alpha|\mathbf{x}_{ij}|)}{|\mathbf{x}_{ij}|^2}\right)\frac{\mathbf{x}_{ij}}{|\mathbf{x}_{ij}|} - \frac{1}{2}\sum_{\mathbf{k}\neq 0}\sum_{j=1}^{N}\frac{q_i q_j}{L_x L_y L_z \kappa^2 \varepsilon_0} e^{-(\kappa^2/4\alpha^2)} i\boldsymbol{\kappa} e^{i\boldsymbol{\kappa}\cdot\mathbf{x}_{ij}}, \quad (6)$$

where q_i are the charges, $\mathbf{x}_{ij}$ is the vector between the position of the ith and jth atoms, and $\boldsymbol{\kappa}$ is a wave number vector indexed by $\mathbf{k}$. The first term in (6) was computed directly using a cutoff of $2.75\sigma_{\max}$. The second term was computed on the mesh using fast Fourier transforms. The α parameter, which regulates the relative contributions from the two sums, was set based on numerical experimentation to be $\alpha = 0.26\,\text{Å}^{-1}$.

C. Flow parameters

The channel dimensions are shown in Fig. 1. The $L_x = L_z = 70\,\text{Å}$ dimensions given in the figure are the periodicity lengths in x and z. The given channel height, $L_y = 65.3\,\text{Å}$, is measured between the centers of the wall atoms. The mean wall charge density was $Q_0 = 0.0817\ \text{C/m}^2$, which is $0.0625e$ per wall atom. This high but physically realizable wall charge was selected because it gives a relatively large number of counterions in the fluid and thus provides a good statistical sample within a reasonable computational time. Still, there were only 50 chlorides dissolved in the 9998 waters in the channel. Each wall was constructed from 400 Lennard-Jones atoms, 1 out of 16 of which was charged with e in the discretely charged wall case. In the other case each wall atom had charge $0.0625e$. In both cases the net charge was zero. The applied electric field acted on each Cl^- in the x direction with $F_E = 2.42\times 10^{-11}$ N. This force is large but necessary to drive the flow at high enough speed to converge velocity statistics.

D. Simulation procedure

To equilibrate the ion distributions, an initial simulation was run with only 7712 atoms, approximately one-quarter the eventual number. There were 2500 waters, 12 Cl^-, and 200 (total) wall atoms. It was initialized with an approximately uniform distribution of Cl^- and was run for 1 million time steps (1 ns) to obtain a statistically stationary chloride distribution. At this point the domain was doubled in both the x and z directions by adding periodic images. The initial simulation had uniformly distributed partial charges on the wall atoms, but now two of the waters were replaced with Cl^- to allow a more nearly uniform distribution of elementary charges on the walls. The charged atoms were arranged to minimize their mutual interaction energy. After this quadrupling procedure, all fluid molecule positions were perturbed by uniformly distributed random displacements with peak amplitude 10^{-3} Å. Because the system is Lyapunov unstable, this small randomization rapidly broke the symmetries. Sixteen different randomized atomic positions were used as initial conditions for 16 separate ensembles that ran simultaneously to accumulate statistics. For each ensemble, 100 000 time steps were used to re-equilibrate and allow the different ensembles to develop away from their similar initial conditions. This was followed by 400 000 time steps to converge statistics.

A Berendsen thermostat was used to counter viscous heating and a small temperature drift associated with the P^3M scheme, which is accurate but not exactly energy conserving. Velocities were rescaled as

$$\tilde{\mathbf{v}}_i = \chi \mathbf{v}_i, \quad (7)$$

where

$$\chi = \left[1 - \frac{\Delta t}{\tau}\left(\frac{T_{\text{tar}}}{T} - 1\right)\right]^{1/2}, \quad (8)$$

and T is the temperature, Δt is the numerical time step (1 fs), T_{tar} is the target temperature (300 K), and τ is a parameter to regulate the strength of the rescaling. Solutions were shown to be insensitive to the value of τ. The mean scaling factor $\overline{\chi}$ was nearly unity: $|\overline{\chi} - 1| < 2\times 10^{-6}$. Since the instantaneous χ was rarely out of the range $0.9995 < \chi < 1.0005$, and 95 percent of the times was within 0.0001 of unity, it did not alter the dynamics significantly. A difficulty arises in applying thermostats when there is a mean flow because the mean flow must be known *a priori* for its kinetic energy to be distinguishable from the thermal kinetic energy. The problem is that the mean is not available until the simulation has run long enough to compute it. Nevertheless, it was found in the present case that results were insensitive to the parabolic flow profile used to estimate the relative contributions, which is no surprise since the mean flow only has a peak velocity of less than 10 m/s and thus constitutes only a tiny fraction of the total kinetic energy of the particles. In atomistic simulations the time step must be short enough to track the velocities of atoms, which for ordinary temperatures and atomic masses are $\sim 10^3$ m/s. Unfortunately, these high atomic velocities make it difficult to converge mean flow statistics when mean flows are typically many times (often several orders of magnitude) smaller than the thermal velocities. Thus, seemingly unphysical flow velocities must be used to increase this signal-to-noise ratio. Couette flow tests showed that the SPC/E viscosity was independent of shear rate to considerably higher shear rates than in the present simulations. Ideally, one should remove heat via the walls, which is the mechanism in a real channel. This has been done for small atomic systems with simple fluids[9] to reduce any unphysical artifacts associated with the thermostat, but this approach does not provide a rigid control of the temperature in the channel. We also note that (7) should technically be applied separately at different distances from the wall because shear and its viscous heating are not uniform across the channel. However, application of a single thermostat for the whole channel in the present case resulted in the desired uniform temperature of 300 K across the channel as seen in Fig. 2. Pressure was regulated to be 1 atmosphere by adjusting the volume of the domain.

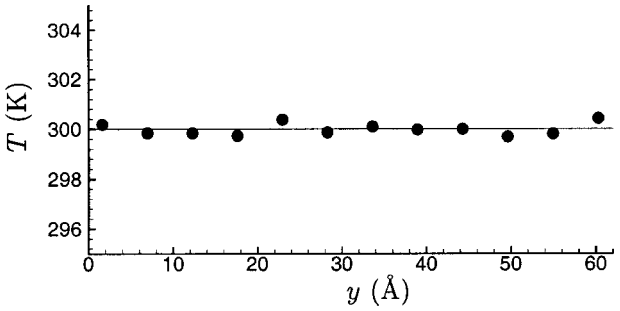

FIG. 2. Mean temperature profile. On this and all plots, $y=0$ corresponds to the centers of the atoms that constitute the lower wall.

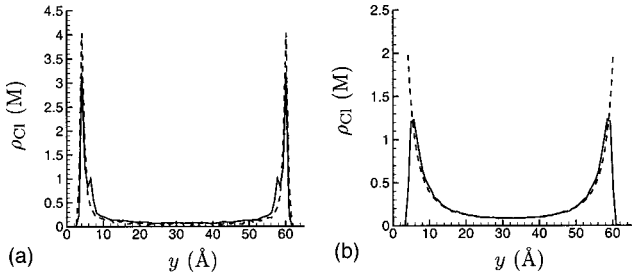

FIG. 4. Ion concentrations. (a) Monte Carlo simulation with Lennard-Jones wall–Cl^- interaction ---; atomistic simulation ———. (b) Monte Carlo simulation with only the repulsive part of the Lennard-Jones potential ——; Poisson-Boltzmann theory (1) ------. In all simulations the walls have distributed ions with elementary charges.

III. RESULTS

A. Ion distribution

Figure 3 shows the Cl^- concentration as a function of distance from the wall. As expected, the profile is sharply peaked near the walls and falls to a low value by the middle of the channel. The small bumps near the peak at both walls result from molecular stacking (see Sec. III B). They are roughly one water molecule width away from the peak.

We see that the profiles for the discretely and uniformly charged walls differ, the uniformly charged wall having more chlorides immediately adjacent to it than the discretely charged wall (see the peak values given in the figure caption). This deficit is balanced by a greater concentration of chlorides just one monolayer further away from the wall. Beyond this very near-wall region, the concentration profiles are nearly the same.

Both the computed profiles differ from the Poisson–Boltzmann prediction of (1) with $\phi(y)$ from (3). To compute the distribution, condition (4) was applied so that the concentration peaks would coincide with those from the simulation. However, the concentration peaks are higher at the walls for the atomistic simulations and fall away faster into the channel.

Monte Carlo simulations of the ionic distribution in absence of the water molecules are used to examine two possible causes of the discrepancy: a deviation of permittivity $\varepsilon\varepsilon_0$ near the wall or wall–fluid dispersion attraction. A standard Metropolis method was used. Figure 4(a) compares the ion distribution in the atomistic simulation discussed above and a Monte Carlo simulation with the water's dielectric effect modeled simply by $\varepsilon=80$. This simulation included the Lennard-Jones potentials as specified in Table I. We see that the two curves agree well, though the peak next to the wall is about 20 percent higher in the Monte Carlo result. There is also no second peak in the Monte Carlo simulation, but one is not expected since it is due to the near-wall structure of the water molecules (see Sec. III B).

The result of a Monte Carlo simulation that includes only the repulsive part of the Lennard-Jones potentials is shown in Fig. 4(b). It agrees well with the Poisson–Boltzmann prediction except near the walls, where finite ion effects become significant. Clearly the dispersion interaction is important.

B. Near-wall water structure

It is expected that the regular structure of the wall will impose a regular structure on the liquid molecules adjacent to it. Figure 5 shows that an ordering persists for approximately three monolayers into the channel. The ordering is stronger for the case with uniformly charged wall atoms. The

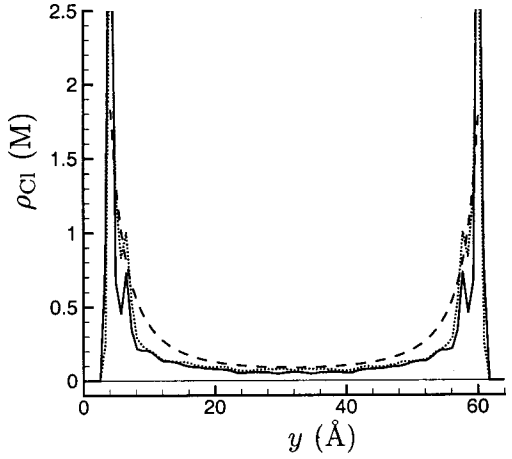

FIG. 3. Chloride number density: ———simulation with uniformly charged wall atoms (peak was $\rho_{Cl}=4.17$ M); ··· simulation with discrete wall atom charges (peak was $\rho_{Cl}=3.21$ M); and --- (1) with ϕ from Poisson–Boltzmann theory (3).

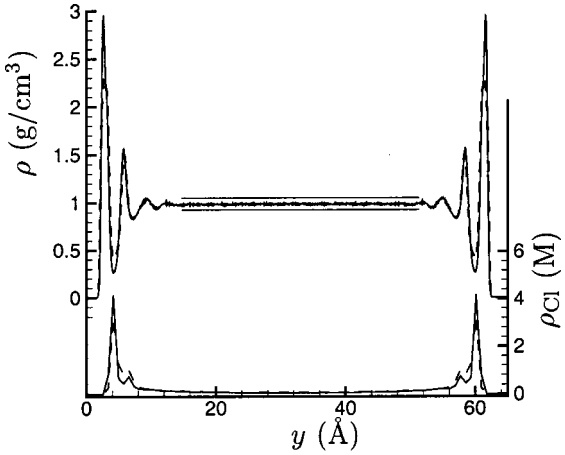

FIG. 5. Water density: ———uniformly charged wall; --- discrete wall charges. The chloride density is shown on the right axis for reference.

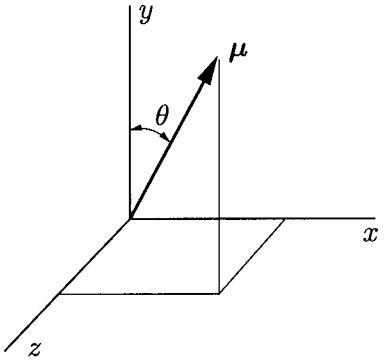

FIG. 6. Schematic defining θ as the angle that the dipole vector $\boldsymbol{\mu}$ makes with the y axis.

chlorides tend to fall between layers of the waters in this region, leading to the secondary peaks we saw in Fig. 3.

Since the wall is charged, we expect there to be a preferred orientation of the water molecules adjacent to it, which will in turn alter their dielectric properties since they cannot respond to an electric field as they do in bulk. With the dipole angle θ defined as in Fig. 6, Fig. 7 shows the probability density function of the angular orientation of the waters at different distances from the wall. The distributions are weighted so that a random orientation gives a uniform distribution. We see that the distribution changes significantly and rapidly near the wall. In the sampling bin centered at $y=1.74$ Å, nearly all the waters have $\theta<90°$, though only the uniformly partially charged wall case has its most probable angle near $\theta=0$. By $y=3.34$ Å, the most probable angle is $\theta\approx 45°$ and both cases are nearly identical. For y between 4 and 5 Å the most probable angle is $\theta=0$. Beyond $y\approx 5$, the distribution slowly flattens and becomes linear. If there is to be any significant change in the dielectric properties of the water due to preferential orientation, it will be confined to a very narrow layer near the wall. We saw in Sec. III A that Monte Carlo simulation with $\varepsilon=80$ was reasonably accurate, though variation of ε might explain the remaining discrepancy in Fig. 4(a).

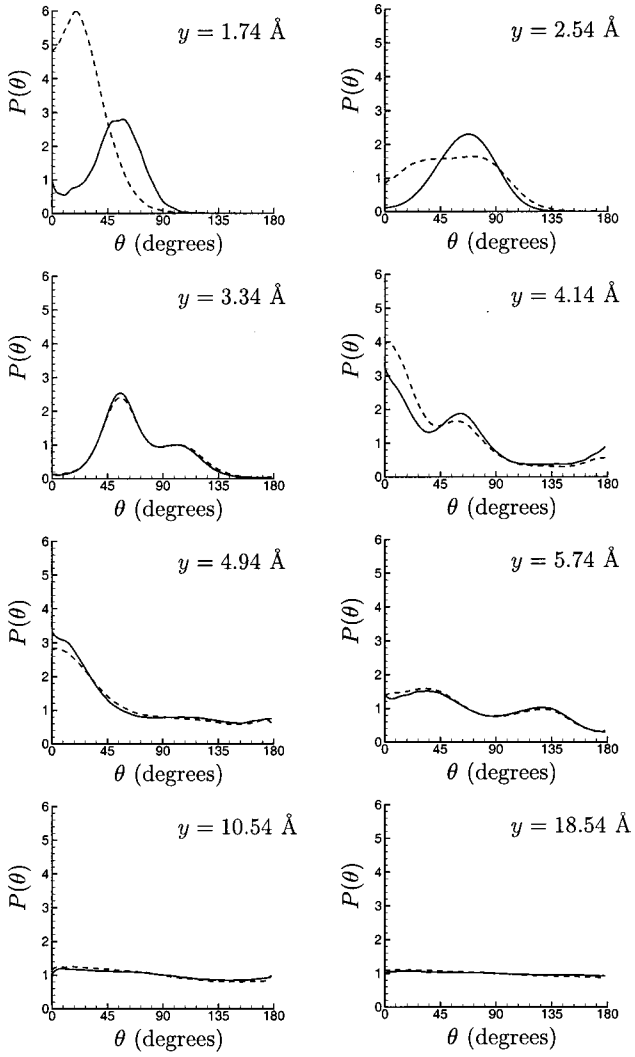

FIG. 7. Probability density function of water molecule orientations:——— discrete distributed wall charge; --- uniformly charged wall atoms. The angle θ is defined in Fig. 6 and the distribution is normalized so that a random distribution will give unity at all angles. The y locations correspond to the center of the oxygen atom.

C. Flow velocity

The computed velocity profiles for both cases are shown in Fig. 8. We see that they are approximately parabolic in the middle of the channel, but do not continue as a parabola all the way to the wall as one would expect for constant-μ Poiseuille flow. Instead, there is considerably more resistance close to the wall. For the simulation with uniformly distributed partial charges, the fluid atoms immediately adjacent to the wall atoms appear fixed in a Stern layer. However, for the case with distributed elementary charges, the velocity drops continuously toward the wall, giving the profile a bell-like shape. In interpreting these results we should note that the strength of the electric field necessary to force a flow velocity large enough to converge velocity statistics might preclude the existence of a finite Stern layer. The existence of a yield stress of the near-wall fluid, a necessary condition for the existence of a Stern layer, has been deduced in experiments that are reviewed by Dukhin and Derjaguin,[10] but our applied force is stronger than that thought necessary to free the wall layers so we should not expect this behavior. However, we will see in the following section that the effective viscosity in this region is well above the accepted bulk value for water, indicating that the wall does indeed increase the viscosity even above the yield stress.

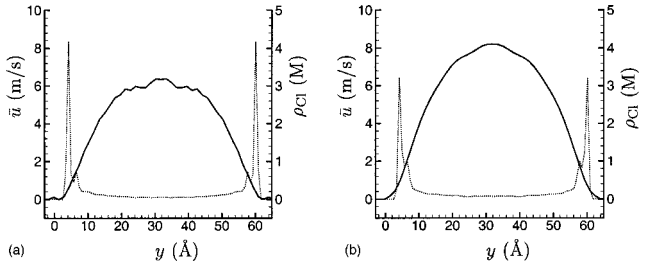

FIG. 8. The mean flow velocity across the channel ———. The mean chloride density is shown on the right axis ⋯. (a) Uniformly charged wall atoms, and (b) discretely charged wall atoms.

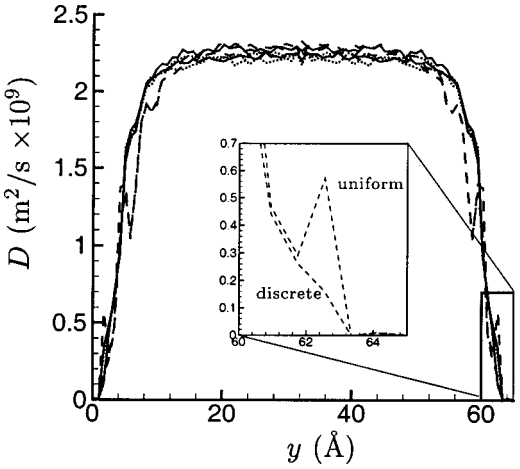

FIG. 9. Diffusivity based on linear fit of mean-squared displacement for 2 ps: ——— D_x, --- D_y, and $\cdots$ D_z. Both the uniformly distributed and discrete unit charge cases are shown and are typically indistinguishable except in the inset plot.

Even if the wall layer is not fixed, diffusivity should decrease in this region. This is the case as seen in Fig. 9, which shows the water self-diffusivity in each of the three coordinate directions as estimated by a linear fit to the mean-square displacement profile after 2 ps

$$D_\alpha = \frac{1}{2}\frac{d\langle \Delta_\alpha^2 \rangle}{dt}, \tag{9}$$

where $\langle \Delta_\alpha^2 \rangle$ is the mean-squared displacement in direction $\alpha = x$, y, or z and D_α is the corresponding diffusivity in that direction. The mean flow begins to bias the mean-squared displacement for times much longer than 2 ps. For $y > 10$ Å $D_x \approx D_y \approx D_z \approx 2.3\times 10^{-9}$ m^2/s, which is close to the accepted value 2.4×10^{-9} for bulk water.[11] Near the wall all the diffusivities drop significantly. The D_x and D_z profiles are essentially identical and independent of the wall charge distribution (both are shown). The y diffusivity follows a similar trend but does not decrease monotonically like the other two. The only significant difference for D_y between the two cases is shown in the figure inset: the uniformly distributed partial charge case has an extra bump, presumably due to the greater near-wall ordering observed in that case. Comparing with Fig. 5, we see that the diffusivity only becomes zero in regions where there are no water molecules.

D. Viscosity

To compute the viscosity, the mean velocity profile was first smoothed by replacing the average value in each bin by the equally weighted mean of that bin and its two nearest neighbors. (There were 81 bins across the channel.) The profile was then fitted by

$$u_{\text{fit}}(y) = u_m \exp\left[\frac{(y-y_m)^4}{y_1^4}\right] + \sum_{n=0}^{11} a_n \cos\frac{\pi y n}{L}, \tag{10}$$

where $u_m = \overline{u}(y_m)$, the peak velocity. First, y_1 was determined so that the exponential term provided the best L_2 fit of the data. Then, the coefficients of the cosine series were least-squares fitted to the difference. The resulting curve and the smoothed data are shown in Fig. 10(a). The fit is seen to be very good.

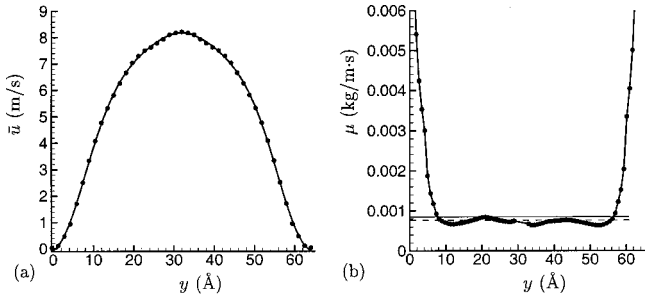

FIG. 10. (a) Mean velocity • fitted by (10) ———. (b) Dynamic viscosity μ computed by (11). The horizontal ——— line is the experimental value for bulk water, and --- is the value for our Couette flow at a range of higher strain rates.

Given a smooth velocity profile (10), the viscosity is easily computed by integrating the Stokes equation (5) in y, which gives

$$\mu(y) = -\frac{\int_{y_m}^{y} n(y')F_E\, dy'}{\dfrac{du_{\text{fit}}}{dy}}. \tag{11}$$

Unfortunately, a numerical evaluation of this fraction is poorly behaved near $y = y_m$ where the numerator and denominator both approach zero, so for clarity points near $y = y_m$ are omitted from Fig. 10(b), which shows $\mu(y)$. We see that the μ profile is reasonably flat for most of the channel, but rises starting at about 10 Å from the walls. Any model that assumes a linear stress–strain relation, such as a simple constant-viscosity Newtonian fluid or a Bingham plastic, which has been used to model the constitutive relation in the past,[10] would not be accurate for the present flow conditions.

The details of the waviness in the viscosity profile in the middle of the channel in Fig. 10(b) are sensitive to the number of terms used in (10), a sensitivity that is amplified by the differentiation in the denominator of (11). However, neither the general form of the curve nor the behavior as the walls are approached is sensitive to the curve-fitting procedure. The value away from the wall is about 10 percent lower than that for pure water, but matches the results for a Couette flow with pure SPC/E water. The equilibrium simulation of Smith and van Gunsteren[12] showed this level of agreement, but was somewhat sensitivity to the parameters used in their reaction field model for long-range Coulomb interactions. This Couette flow was simulated at various strain rates, all higher than in the present flow, and μ was shown to be strain-rate independent.

IV. SUMMARY

We found that the ion distribution in the atomistic simulation was in general agreement with the Poisson–Boltzmann theory away from the wall, but ions were more attracted to

the wall than this theory predicted. Monte Carlo simulations using constant $\varepsilon = 80$ predicted a distribution similar to that observed in the dynamic simulation, suggesting that any deviations in the permittivity due to the observed ordering of the waters adjacent the wall, even in this highly charged wall case, do not significantly affect the ion distributions. Similar Monte Carlo simulations that neglected the attractive component of the Lennard-Jones wall$-Cl^-$ interaction predicted a distribution close to that predicted by the Poisson–Boltzmann theory. Clearly, the dispersion interaction with the wall is important for the parameters chosen.

The velocity was found, as expected, to be approximately parabolic in the middle of the channel, but it flattened out near the walls in a Stern-type layer, though the molecules immediately adjacent to the wall were not completely fixed. They had essentially zero mean streamwise velocity in the first layer only for the case of uniformly distributed partial charges. Self-diffusivity of the waters decreased significantly in the region, but did not become zero. Viscosity increased substantially in this layer, rising by over a factor of 6 in the 10 Å closest to the wall.

[1] J. Israelachvili, *Intermolecular and Surface Forces* (Academic, New York, 1992).
[2] R. J. Hunter, *Zeta Potential in Colloid Science* (Academic, London, 1981).
[3] A. E. Herr, J. I. Holho, J. G. Santiago, M. G. Mungal, and T. W. Kenny, ''Electro-osmotic capillary flow with nonuniform zeta potential,'' Anal. Chem. **72**, 1053 (2000).
[4] D. Coelho, M. Shapiro, J.-F. Thovert, and P. Adler, ''Electro-osmotic phenomena in porous media,'' J. Colloid Interface Sci. **181**, No. 1, 169 (1996).
[5] H. J. C. Berendsen, J. R. Grigera, and T. P. Straatsma, ''The missing term in effective pair potentials,'' J. Phys. Chem. **91**, 6269 (1987).
[6] J. Chandrasekhar, D. Spellmeyer, and W. Jorgensen, ''Energy component analysis for dilute aqueous solutions of Li+, Na+, F−, and Cl− ions,'' J. Am. Chem. Soc. **106**, 903 (1984).
[7] E. Pollock and J. Glosli, ''Comments on PPPM, FMM, and the Ewald method for large periodic Coulombic systems,'' Comput. Phys. Commun. **95**, 93 (1996).
[8] R. W. Hockney and J. W. Eastood, *Computer Simulation using Particles* (American Institute of Physics New York, 1988).
[9] K. P. Travis and K. E. Gubbins, ''Poiseuille flow of Lennard-Jones fluids in narrow slit pores,'' J. Chem. Phys. **112**, 1984 (2000).
[10] S. S. Dukhin and B. V. Derjaguin, *Surface and Colloid Sciences* (Wiley, New York, 1974), Vol. 7, pp. 49–272.
[11] *CRC Handbook of Chemistry and Physics*, edited by D. R. Lide (CRC, Cleveland, 1994).
[12] P. E. Smith and W. F. van Gunstersen, ''The viscosity of SPC and SPC/E water at 277 and 300 K,'' Chem. Phys. Lett. **79**, No. 2, 926 (1983).